Effect of Pressure Relaxation on the Mechanisms of Short-Pulse Laser Melting

Dmitriy S. Ivanov and Leonid V. Zhigilei

Department of Materials Science & Engineering, University of Virginia, 116 Engineer's Way, Charlottesville, Virginia 22904-4745, USA

(Received 4 March 2003; published 4 September 2003)

The kinetics and microscopic mechanisms of laser melting of a thin metal film are investigated in a computational study that combines molecular dynamics simulations with a continuum description of the laser excitation and subsequent relaxation of the conduction band electrons. Two competing melting mechanisms, homogeneous nucleation of liquid regions inside the crystalline material and propagation of melting fronts from external surfaces, are found to be strongly affected by the dynamics of the relaxation of the laser-induced pressure.

DOI: 10.1103/PhysRevLett.91.105701 PACS numbers: 64.70.Dv, 02.70.Ns, 61.80.Az, 79.20.Ds

Although melting is a common and well-studied phenomenon, the nature of the structural instability of a superheated crystal and the microscopic mechanisms of melting are still subjects of active scientific discussions [1–3]. Recent experimental investigations combining short pulse laser irradiation with optical, x-ray, and electron diffraction time-resolved probe techniques [4–7] have a promise of providing new insights into the melting mechanisms and kinetics. The extremely high heating rates of 10^{14} K/s and even more can be achieved by short (pico- and femtosecond) pulse laser irradiation, opening unique opportunities for investigation of the kinetic limits of achievable superheating. While the time-resolved pump-probe experiments are providing valuable information on the time scales of the laser-induced melting, a reliable interpretation of the experimental observations requires a better understanding of the microscopic mechanisms of melting occurring under highly nonequilibrium conditions created in the target material by short pulse laser irradiation. In this Letter we report the results of a molecular dynamics (MD) simulation study of short pulse laser melting of a thin metallic film. Simulation results provide insights into the atomic-level mechanisms of laser melting and, in particular, reveal a strong effect of the laser-induced pressure on the melting process.

A hybrid computational model that combines classical MD method for simulation of nonequilibrium processes of lattice superheating and ultrafast melting with a continuum description of the laser excitation and subsequent relaxation of the conduction band electrons is used in the simulations. The model is based on so-called two-temperature model (TTM) [8], which describes the time evolution of the lattice and electron temperatures, T_l and T_e, by two coupled nonlinear differential equations. In the combined TTM-MD method [9–11], MD substitutes the TTM equation for the lattice temperature. The equation for the electron temperature is solved by a finite difference method simultaneously with MD integration of the equations of motion of atoms. The electron temperature enters a coupling term that is added to the MD equations of motion to account for the energy exchange between the electrons and the lattice. A modified, as compared to earlier works [9,10], formulation of the coupling term is used in the model. The new formulation distinguishes between the thermal velocities of the atoms and the velocities of their collective motion. It also does not require *a priori* knowledge of the lattice heat capacity of the model system, which is, in general, a function of temperature. The expansion, density variations, and, at higher fluences, disintegration of the irradiated target predicted in the MD part of the model are accounted for in the continuum part of the model. A complete description of the combined TTM-MD model is given elsewhere [11].

The simulation reported in this Letter is performed for a 50 nm freestanding Ni film irradiated with a 200 fs laser pulse at an absorbed fluence of 430 J/m^2. Simulations for Ni and Au films performed at different fluences and pulse durations from 200 fs to 200 ps support the conclusions made in this Letter and are reported elsewhere [11]. The parameters used in the TTM equation for the electron temperature are as follows [12]. The electronic heat capacity is $C_e = AT_e$ with $A = 1065\,\mathrm{J m^{-3} K^{-2}}$, the thermal conductivity of the electrons is $K_e = K_0 T_e / T_l$ with $K_0 = 91\ \mathrm{W m^{-1} K^{-1}}$, the electron-phonon coupling constant is $G = 3.6 \times 10^{17}\ \mathrm{W m^{-3} K^{-1}}$, and the optical absorption depth is $L_p = 13.5$ nm. The initial MD system is an FCC crystal composed of 56 800 atoms with dimensions $3.53 \times 3.53 \times 50.14$ nm and periodic boundary conditions imposed in the directions parallel to two (100) free surfaces. Interatomic interaction is described by the embedded-atom method (EAM) in the form suggested in Ref. [13]. Before applying laser irradiation, the system is equilibrated at 300 K and zero pressure.

The lattice temperature contour plot shown in Fig. 1(a) reflects the complexity of the material response to the short pulse laser irradiation. There are several processes that are responsible for the evolution of the lattice temperature distribution in the irradiated film. First, the energy transfer from hot electrons to the lattice leads to the initial temperature increase. Strong electron-phonon coupling in Ni results in the development of a temperature gradient within the 50 nm film, Fig. 1(a).

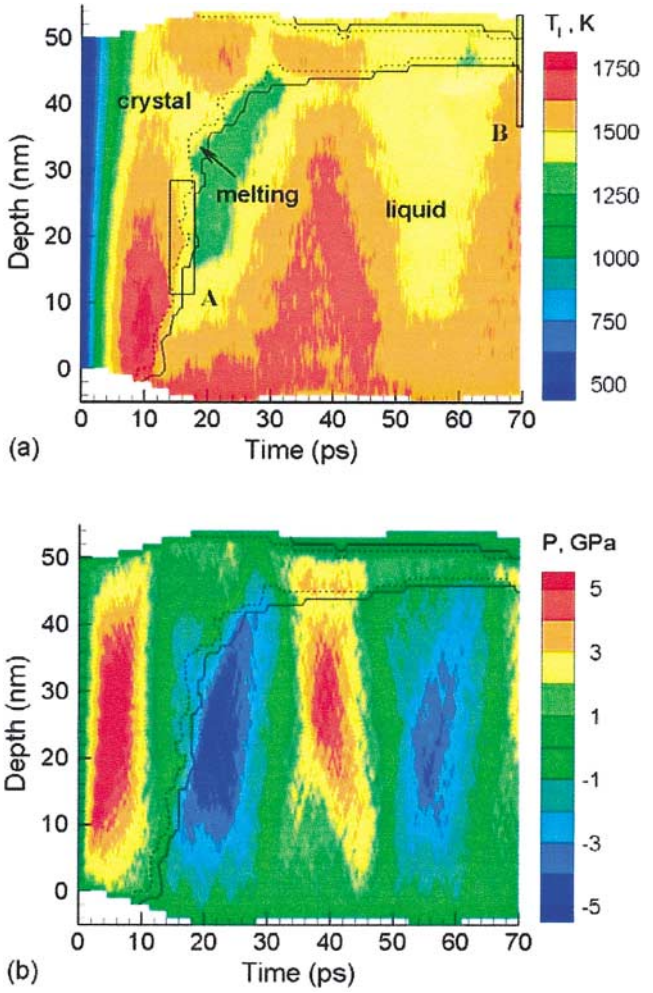

FIG. 1 (color). Contour plots of lattice temperature (a) and pressure (b) for simulation of laser melting of a 50 nm Ni film irradiated with a 200 fs laser pulse at an absorbed fluence of 430 J/m^2. Solid and dashed lines show the beginning and end of the melting process. Rectangles A and B in (a) show the areas of the film and times for which snapshots are shown in Fig. 3. Laser pulse is directed along the Y axes, from the bottom of the contour plots.

The second factor affecting the temperature is the onset of melting, which leads to a transient decrease of the lattice temperature due to the transfer of a part of the thermal energy to the latent heat of melting. The effect of melting on the lattice temperature can be seen in Fig. 1(a), where the dashed and solid lines show the beginning and the end of the melting process, respectively. The dashed line goes through the regions in the film where 10% of atoms have a "liquidlike" environment (as defined by the local order parameter [11]), whereas the solid line connects the regions where 90% of atoms belong to the liquid phase.

The third factor that has a significant effect on the long-term temperature evolution is the relaxation of the laser-induced pressure in the irradiated film. Strong electron-phonon coupling in nickel leads to the steep rise of the lattice temperature during the first ~5 ps after the laser pulse, Fig. 1(a). This time is shorter than the time needed for the film to expand in response to the corresponding thermoelastic stresses and, in the central part of the film, the heating takes place under condition of the inertial stress confinement [15]. The heating under the condition of stress confinement results in the buildup of a high, up to 7.7 GPa, compressive pressure, Fig. 1(b). Relaxation of the compressive pressure leads to the expansion of the freestanding film with tensile stresses concentrating in the central part of the film. The following gradually dissipating oscillations of the film continue beyond the time of the simulation. A direct correlation between the pressure and temperature variations in the film is apparent from comparison of Figs. 1(a) and 1(b). Compression leads to the temperature increase whereas expansion corresponds to cooling. Neglecting viscosity and dissipation of the energy of the elastic oscillations and considering the compression and expansion as isentropic processes, the temperature variation with pressure can be estimated from thermodynamics, $(\partial T/\partial P)_S = VT\alpha/C_P$. In order to integrate this equation, we calculated the pressure and temperature dependence of the heat capacity C_P, volume V, and the volume coefficient of thermal expansion α for the EAM Ni material in both solid and liquid states. The results of the integration for the crystal phase are shown in Fig. 2 by blue dashed lines. Similar slopes of the isentropes are observed for the liquid phase. For a pressure variation from about -5 to about 4 GPa, observed after ~35 ps in the central part of the film in Fig. 1(b), the range of the temperature variation of ~200 K is predicted for the isentropic expansion or compression. This prediction correlates well with the temperature variation observed in Fig. 1(a).

Turning to the analysis of the mechanisms of laser melting, we can see from Fig. 1(a) that the melting process occurs in two steps. An ultrafast melting of ~80% of the film occurring within ~15 ps is followed by a much slower melting of the remaining crystalline region near the back surface of the film that takes more than 100 ps. The irradiated side of the film starts to melt ~10 ps after the laser pulse, when the temperature reaches ~1650 K, significantly above the equilibrium melting temperature of 1439 K, determined for the EAM Ni from a liquid-crystal coexistence simulation at zero pressure. Although, at first sight, the melting seems to proceed by propagation of the melting front from the irradiated surface, a closer look at a series of snapshots of the atomic-level structure of a region undergoing ultrafast melting, Fig. 3(a) and [14], reveals a more complex picture characteristic of homogeneous melting. Small liquid regions appear and grow ahead of the "melting front" leading to a very high apparent melting front propagation velocity of ~4000 m/s.

While the ultrafast homogeneous melting starts near the irradiated surface under conditions of strong overheating, in the central part of the film it proceeds at significantly lower temperatures. This observation can be

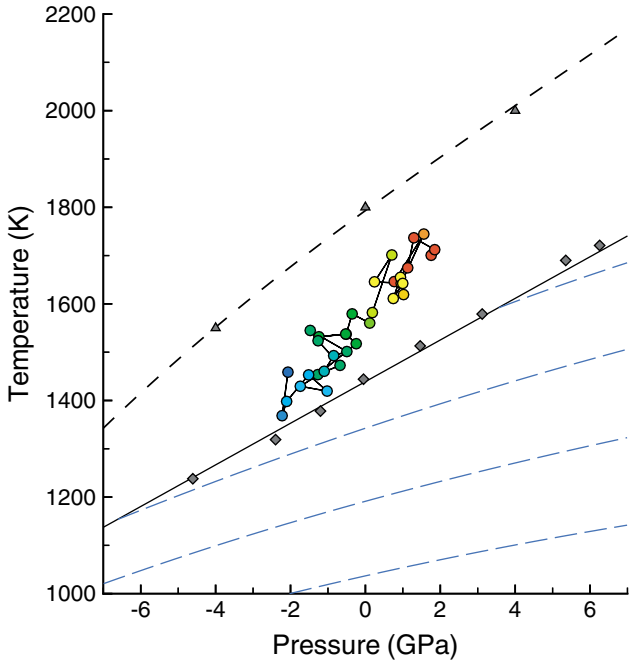

FIG. 2 (color). Conditions of equilibrium and nonequilibrium melting observed in simulations performed for EAM Ni material. Dark diamonds correspond to the conditions of equilibrium melting obtained in liquid-crystal coexistence simulations. The slope of the solid line is calculated from the Clapeyron equation. Blue dashed lines are isentropes plotted for four different values of entropy. Dark triangles connected by the black dashed line correspond to the maximum overheating of crystal observed in simulations performed with 3D periodic boundary conditions. Color circles show the conditions leading to the onset of homogeneous melting in the simulation of laser melting. The conditions for the onset of homogeneous melting are realized along the dashed line in Fig. 1 for the depth up to 35 nm. The circles are connected by lines and colored from red to blue in the order of increasing depth under the surface.

explained based on the pressure dependence of both the equilibrium melting temperature and the temperature of maximum overheating shown in Fig. 2. A series of liquid-crystal coexistence simulations performed at different pressures predicts a nearly linear dependence of the equilibrium melting temperature on pressure. This prediction is in a good agreement with calculations based on Clapeyron equation, $(dT/dP)_m \approx \Delta V_m/\Delta S_m$. For the model EAM Ni material, the values of volume and entropy of melting at zero pressure are found to be $\Delta V_m = 0.46$ cm^3/mol and $\Delta S_m = 10$ J/K-mol. Both ΔV_m and ΔS_m decrease with increasing pressure, leading to a weak nonmonotonous pressure dependence of the slope of the coexistence line with an average value of $(dT/dP)_m \approx 45$ K/GPa.

The temperature and pressure conditions leading to the onset of the ultrafast homogeneous laser melting are shown in Fig. 2 by color circles. These conditions are calculated along the dashed line in Fig. 1 for the depth under the irradiated surface up to 35 nm. At all pressures, the homogeneous melting starts under conditions of overheating above the liquid-crystal coexistence line. The overheating required for initiation of the homogeneous melting in this simulation is found to range from less than $1.05\,T_m$ to $1.18\,T_m$. These values are significantly lower then the temperatures at which homogeneous melting is observed in constant-pressure simulations performed with three-dimensional periodic boundary conditions, 1.21–$1.25\,T_m$, shown by triangles connected by the black dashed line in Fig. 2. The temperature needed to initiate melting in a system with no external boundaries and internal defects corresponds to the limit of thermal stability of the crystal lattice [2], and can be considered as the maximum possible overheating achievable in a system. The discrepancy between the maximum overheating under constant-pressure conditions and the one required for the initiation of homogeneous melting under the short pulse laser irradiation conditions can be explained by the dynamics of the relaxation of the laser-induced pressure. The strong pressure gradients transiently realized in the irradiated films, Fig. 1(b), and associated complex stress conditions can destabilize the lattice and promote melting at lower overheatings. Moreover, for a typical laser spot diameter of 10–100 μm the fast relaxation of the laser-induced pressure can only proceed in the direction normal to the surface. This uniaxial expansion and associated anisotropic lattice distortions can additionally reduce the lattice stability against the initiation of melting. Indeed, the melting process in the simulation proceeds simultaneously with the uniaxial expansion of the film, Fig. 1(b), leading to the decrease of the overheating needed for the initiation of the homogeneous melting. This is apparent from Fig. 2, where the points corresponding to the onset of the homogeneous melting are approaching the coexistence line as depth (and time) increases. As a result, our simulations suggest that homogeneous melting can be induced at significantly lower values of overheating and a significantly larger range of irradiation parameters as compared to the predictions based on the classical nucleation theory [3].

The overheating achieved in a region near the back surface of the irradiated film is not sufficient to induce homogeneous melting, and a much slower conventional heterogeneous melting takes place there. Two melting fronts propagate from the back surface of the film and from the homogenously melted part of the film, Fig. 3(b), leading to the complete vanishing of the crystalline layer by the time of $\sim$115 ps after the laser pulse [14]. The heterogeneous melting is also affected by the pressure variations. The decrease in the thickness of the crystalline layer coincides with the expansion of the region. This is related to the steeper slope of the coexistence line as compared to isentropes, $(dT/dP)_m > (dT/dP)_S$, Fig. 2. An adiabatic expansion of a region of the liquid-crystal coexistence facilitates melting and induces the advancement of the melting front.

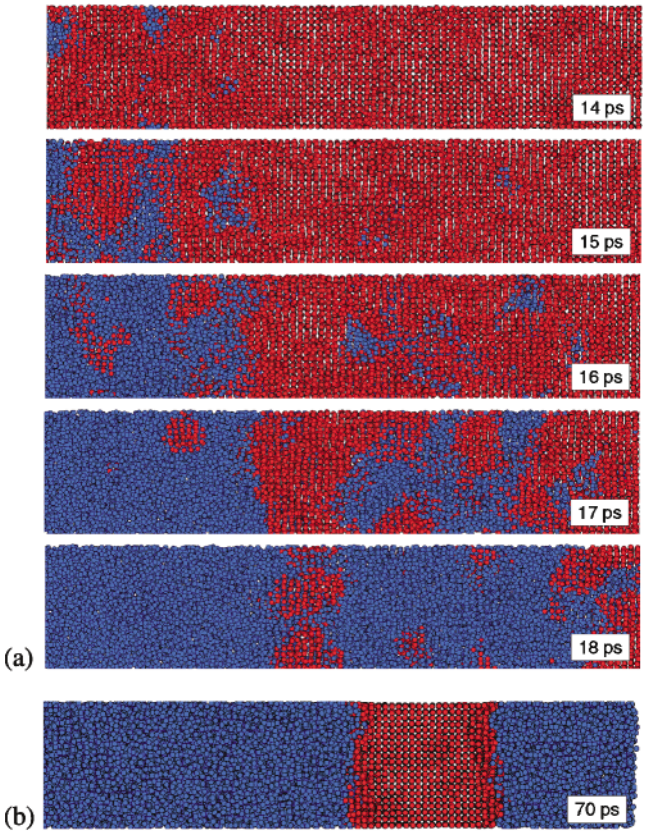

FIG. 3 (color). Snapshots from the simulation of laser melting for times and locations marked by rectangles A (a) and B (b) in Fig. 1(a). Atoms are colored according to the local order parameter—red atoms have local crystalline surroundings, blue atoms belong to the liquid phase. Animated sequences of snapshots from the simulation can be found at [14].

The role of laser-induced pressure in laser melting is defined by pulse duration as well as by the strength of electron-phonon coupling. The maximum values of laser-induced pressure are related to the condition of stress confinement [15] that, for 50 nm films, is satisfied for heating times up to ~10 ps. In particular, in simulations performed for gold films [11] the characteristic time of energy transfer from the excited electrons to the lattice is longer, ~20 ps, as compared to nickel, ~5 ps. As a result, in gold films the laser-induced thermoelastic pressure is significantly weaker, the effect of pressure variations on the kinetics and mechanisms of laser melting is less pronounced and homogeneous nucleation of the liquid phase is observed at conditions closer to the maximum overheating. Similarly, pressure variations are small and do not play any significant role in melting of 50 nm Ni films irradiated with pulses longer than 25 ps [11]. Note, that the effect of the uniaxial thermal expansion is present even in cases of laser irradiation with longer pulses, moderately reducing lattice stability as compared to heating under hydrostatic pressure conditions.

In general, the strong influence of pressure relaxation on melting mechanisms, reported in this Letter for a thin metal film, can be expected for different systems and target materials, as soon as laser heating is fast enough to satisfy the conditions for inertial stress confinement [15] and to generate high compressive pressure. The relaxation of the laser-induced pressure, which takes place due to the presence of free surface(s), proceeds at the same time scale as the melting process and affects the kinetics and mechanisms of melting.

In conclusion, the results of the simulation demonstrate that the interplay of two competing processes, propagation of the liquid-crystal interfaces, and homogeneous nucleation of the liquid phase inside the bulk of the crystal, is responsible for fast melting of a metal film irradiated by a short laser pulse. The dynamics of relaxation of laser-induced pressure has a profound effect on temperature distribution in irradiated films as well as on both homogeneous and heterogeneous melting processes. Homogeneous nucleation of liquid regions inside crystalline material is assisted by anisotropic lattice distortions and stress gradients induced by the fast laser heating. The lattice distortions and stress gradients reduce the overheating required for the initiation of homogeneous melting down to less than $1.05\,T_m$. The reduced lattice stability under conditions of short pulse laser irradiation has important implications for interpretation of experimental data on the kinetics of laser melting.

[1] K. Lu and Y. Li, Phys. Rev. Lett. **80**, 4474 (1998).
[2] Z. H. Jin, P. Gambsch, K. Lu, and E. Ma, Phys. Rev. Lett. **87**, 055703 (2001).
[3] B. Rethfeld, K. Sokolowski-Tinten, D. von der Linde, and S. I. Anisimov, Phys. Rev. B **65**, 092103 (2002).
[4] S. Williamson, G. Mourou, and J. C. M. Li, Phys. Rev. Lett. **52**, 2364 (1984).
[5] B. Lin and H. E. Elsayed-Ali, Surf. Sci. **498**, 275 (2002).
[6] M. B. Agranat *et al.*, Appl. Phys. A **69**, 637 (1999).
[7] K. Sokolowski-Tinten *et al.*, Nature (London) **422**, 287 (2003).
[8] S. I. Anisimov, B. L. Kapeliovich, and T. L. Perel'man, Sov. Phys. JETP **39**, 375 (1974).
[9] H. Häkkinen and U. Landman, Phys. Rev. Lett. **71**, 1023 (1993).
[10] C. Schäfer, H. M. Urbassek, and L. V. Zhigilei, Phys. Rev. B **66**, 115404 (2002).
[11] D. S. Ivanov and L. V. Zhigilei, Phys. Rev. B **68**, 064114 (2003).
[12] J. Hohlfeld *et al.*, Chem. Phys. **251**, 237 (2000).
[13] X. W. Zhou *et al.*, Acta Mater. **49**, 4005 (2001).
[14] See EPAPS Document No. E-PRLTAO-91-052334 for animated sequences of snapshots from the simulation. A direct link to this document may be found in the online article's HTML reference section. The document may also be reached at ftp://ftp.aip.org/epaps/phys_rev_lett/E-PRLTAO-91-052334/index.html
[15] L. V. Zhigilei and B. J. Garrison, J. Appl. Phys. **88**, 1281 (2000).